This is a repository copy of *DQ analysis of fractional-slot machines with star-delta concentrated winding*.

White Rose Research Online URL for this paper:
https://eprints.whiterose.ac.uk/213238/

Version: Published Version

Article:
Rudden, I., Wang, P., Li, H. et al. (4 more authors) (2024) DQ analysis of fractional-slot machines with star-delta concentrated winding. IEEE Access, 12. pp. 84680-84690. ISSN 2169-3536

https://doi.org/10.1109/ACCESS.2024.3413145

Reuse
This article is distributed under the terms of the Creative Commons Attribution (CC BY) licence. This licence allows you to distribute, remix, tweak, and build upon the work, even commercially, as long as you credit the authors for the original work. More information and the full terms of the licence here: https://creativecommons.org/licenses/

Takedown
If you consider content in White Rose Research Online to be in breach of UK law, please notify us by emailing eprints@whiterose.ac.uk including the URL of the record and the reason for the withdrawal request.

eprints@whiterose.ac.uk
https://eprints.whiterose.ac.uk/

This article has been accepted for publication in IEEE Access. This is the author's version which has not been fully edited and
content may change prior to final publication. Citation information: DOI 10.1109/ACCESS.2024.3413145

IEEE Access
Multidisciplinary | Rapid Review | Open Access Journal

Date of publication xxxx 00, 0000, date of current version xxxx 00, 0000.

Digital Object Identifier xxx

DQ Analysis of Fractional-Slot Machines with Star-Delta Concentrated Winding

I. A. Rudden[1], P. Wang[1], H. Li[1], G. J. Li[1], Senior Member, IEEE, Z. Q. Zhu[1], Fellow, IEEE, A. Duke[2], R. Clark[2]

1, Department of Electronic and Electrical Engineering, The University of Sheffield, Sheffield, UK,
2, Siemens Gamesa Renewable Energy Limited, North Campus, Broad Lane, Sheffield, UK

Corresponding author: Guang-Jin Li (e-mail: g.li@sheffield.ac.uk).

This work is supported by the UK EPSRC Prosperity Partnership "A New Partnership in Offshore Wind" under Grant No. EP/R004900/1.

ABSTRACT This paper presents a novel method for addressing the challenge of *dq*-transformation in fractional-slot machines with star-delta connected concentrated windings. These machines have no neutral point, preventing direct measurement of mutual inductance between phases. This complicates the calculation of *d*- and *q*-axis inductances, which are crucial for modern control techniques such as field-oriented and sensorless control. The proposed method derives *d*- and *q*-axis inductances as functions of individual star and delta coil inductances, which can easily be measured. Moreover, it demonstrates that the *d*- and *q*-axis inductances can be calculated using measurements from just two adjacent coils. The method begins with constructing a decomposed coil-by-coil inductance matrix, separating each phase winding into individual star and delta coil inductances. This matrix is then transformed into the *dq*-frame using a three-step process: firstly, summing individual flux linkages to derive line flux linkage based on circuit configuration; secondly, decomposing 3-phase *abc* supply currents into individual currents within the star and delta coils to address phase shift and amplitude differences; and finally, transforming line flux linkage into the *dq*-frame using a modified power-invariant Park transformation. The proposed method is validated by simulations and experiments on both surface mounted and interior permanent magnet machines.

INDEX TERMS *dq* analysis, concentrated windings, fractional-slot, star-delta connection.

I. INTRODUCTION

Machines equipped with fractional-slot concentrated windings (FSCW) offer substantial advantages in manufacturing and torque performance over traditional integer-slot distributed windings [1]. However, they have the disadvantage of large space harmonics in the armature winding MMF [2]. These large space harmonics lead to increased vibrations and torque ripple as well as increased rotor loss and PM eddy current loss [3-5]. The latter is a particular problem for machines operating under high current loading where the increased PM eddy current losses lead to excess heating [6]. This excess heating can cause irreversible demagnetization of the PMs and so methods to mitigate these MMF space harmonics are very attractive [7-10]. There is a wealth of recent research investigating the application of hybrid star-delta windings in FSCW machines as a method for space harmonic elimination [11-15]. In this winding topology one phase group of coils are connected in star, but instead of connecting at the neutral point the ends are connected to the junctions between coils in a delta-connected winding. This configuration creates a 30 elec. deg. phase shift between the two windings that can be used to eliminate unwanted harmonics. Various configurations of hybrid star-delta windings have been proposed in literature that reduce or eliminate unwanted armature MMF harmonics. Abdel-Khalik *et al* demonstrated the application of this type of winding connection to *m*-phase machines in [11]. In this work a 12s/10p 3-phase star-delta wound machine has been investigated and compared with a conventional star winding. It is demonstrated that the star-delta wound machine can eliminate the 1st subspace harmonic while also improving the amplitude of the working (5th) harmonic by 3.5%. This yields a machine with improved torque performance and reduced rotor loss. Hybrid star-delta windings have been extended to a multitude of electrical machine applications including interior permanent magnet (IPM) machines [16] and synchronous reluctance machines [17, 18]. Designing electrical machines to reduce unwanted harmonics and thus improve performance is of vital importance. However, understanding how to control these machines is also critical to their application in the real world. The *dq*-transformation [19] is fundamental to many modern control methodologies including field-oriented control [20] and sensorless control [21, 22]. Although star-delta winding structures possess many advantages such as reduced harmonics and losses, it is difficult to get the *dq*-axis parameters such as L_d and L_q needed for these control schemes. This will be the main focus of this paper.

From an electromagnetic design perspective, a star-delta winding machine can be viewed as a pseudo dual-3-phase machine owing to the phase shift between the currents in the two winding sets. There is a large amount of work on *dq*-analysis of dual 3-phase machines [23]. Many of these methods use a double synchronous reference frame for current control of each winding set based on two individual *dq*-axis models [24-26]. These methods work for steady-state control, however the two individual reference frames may develop instability if there is a large amount of cross-coupling between the winding sets [27]. Therefore, the two *dq*-frames must be decoupled from one another for optimum current control. A general decoupled *dq*-model is proposed in [28] for a PM synchronous generator with isotropic rotor. This method considers the dependence of self- and mutual inductances on rotor position and greatly simplifies the analysis by decoupling the two winding sets. In [29] a simple diagonalization matrix is introduced that can perform the decoupling and takes into account the harmonic content of no-load flux linkages. This provides a general decoupled *dq*-model for dual 3-phase machines but does not account for rotor anisotropy. Finally, work carried out by Kallio *et al* presents a decoupled *dq*-model for dual 3-phase interior

This work is licensed under a Creative Commons Attribution 4.0 License. For more information, see https://creativecommons.org/licenses/by/4.0/

This article has been accepted for publication in IEEE Access. This is the author's version which has not been fully edited and
content may change prior to final publication. Citation information: DOI 10.1109/ACCESS.2024.3413145

permanent magnet (IPM) machines that considers the influence of rotor saliency [30]. This work describes the simple transformations that can be carried out to allow for *dq*-control of dual 3-phase IPM machines with general angle displacements between the winding sets. This approach can then be used to determine inductance parameters for decoupled *dq*-models [31], and to develop high-performance control for dual 3-phase PM machines in different reference frames [32].

These prior works are all very useful. However, they cannot be applied in the case of a hybrid star-delta wound machine. In such a machine, although the winding sets behave as if driven by two converters, they are connected in series. This means that there is only one converter used to drive the windings and so two decoupled *dq*-reference frames cannot be employed. A control scheme must be generated that accounts for the phase shift in the two winding sets but still produces only a single *dq*-frame for *dq*-analysis. There is presently no literature investigating the *dq*-inductances and therefore *dq*-analysis of star-delta machines. This could be due to the fact that the bulk of literature on star-delta machines is applied to non-salient pole rotors. In this case there is no rotor anisotropy which causes complex cross-coupling between individual coils. Thus, in such machines a simple star-delta transformation of fundamental inductance could be applied to generate a simplified *dq*-inductance. However, in an IPM machine the inductance becomes a function of rotor position. This can also be the case for some of the surface mounted permanent magnet (SPM) machines when the saturation induced saliency is accounted for. If there is a phase-shift between coils within the same phase as well as between phases, then the mutual inductance between each coil must be expressed independently. Furthermore, this simplification would produce *dq*-inductances as a function of phase self- and mutual-inductance. In a star-delta wound machine there is no neutral point, and so measuring these inductances is not possible. Therefore, a decomposed inductance matrix, which can then be translated to the *dq*-frame is required that allows measurement of individual coil self- and mutual-inductances.

In this paper, a method for *dq*-transformation of a star-delta wound machine is proposed. An IPM machine is used as example, but the same theory can be applied to an SPM machine to account for the saliency caused by saturation. A demonstration of this *dq*-transformation process for obtaining *dq* armature flux linkage based on supplied *dq* currents can be seen in Fig. 1. The process begins with the generation or

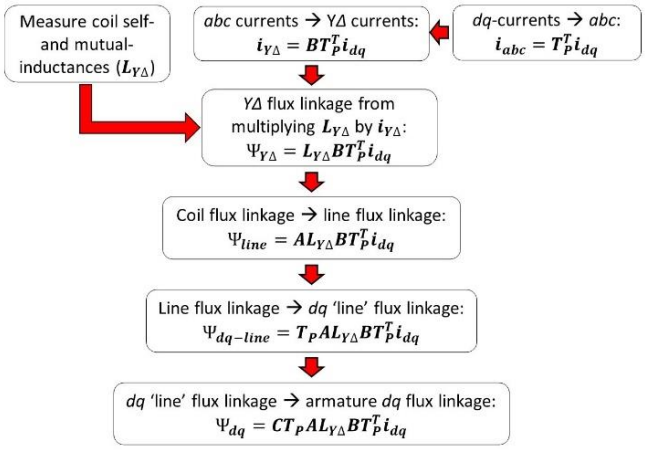

Fig. 1. Flowchart describing process for obtaining *dq* armature flux linkages.

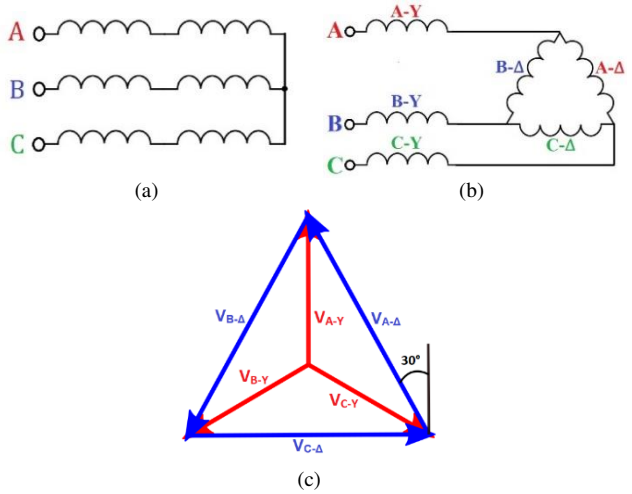

Fig. 2. 3-phase winding connections. (a) Conventional 3-phase windings, (b) star-delta windings, and (c) star-delta winding voltage vectors.

measurement of a decomposed coil-by-coil stator inductance matrix ($\boldsymbol{L_{Y\Delta}}$) that accounts for the mutual inductance between individual star and delta coils. The *d*- and *q*-axis currents are transformed to the *abc* frame by the inverse Park transform ($\boldsymbol{T_P^T}$), and then decomposed into individual star and delta coil currents using a circular matrix ($\boldsymbol{B}$). The coil inductance matrix is then multiplied by the individual coil currents to provide individual star and delta coil flux linkages. These are then summed in such a way to provide the line flux linkage using a matrix ($\boldsymbol{A}$). The line flux linkage is then transformed to a pseudo *dq* 'line' flux linkage with the Park transform ($\boldsymbol{T_P}$) before a final matrix ($\boldsymbol{C}$) transforms it to the final *dq* armature flux linkage. This process can be applied to give the *dq*-voltage equation that can be used for *dq*-control of the star-delta machine, as well as calculation of the *d*- and *q*-axis inductances.

II. Star-Delta Winding Machine

A. Star-Delta Connected Windings

The inherent phase shift between the star and delta coil currents can be used to eliminate the unwanted first subspace harmonic. To exploit this property, the ends of the star windings are connected to the junctions of the delta windings and the difference between a conventional star winding and the star-delta winding can be seen in Fig. 2(a) and Fig. 2(b). The voltage phasors for the star and delta winding sets can be seen in Fig. 2(c), demonstrating the 30 elec. deg. phase shift that exists between the two windings.

It has been demonstrated in literature that this phase shift can be applied to a 12s/10p FSCW machine to eliminate the 1st subspace harmonic while increasing the amplitude of the working (5th) harmonic by 3.5% [11]. In this paper both IPM and SPM machines are investigated, but emphasis on the IPM machine is used in the equation derivations as the influence of rotor saliency on star-delta coil mutual inductance is more significant. The example IPM star-delta machine, as well as the harmonic spectra of the winding MMF, can be seen in Fig. 3 with machine specifications given in TABLE I. The combination of eliminated 1st subspace harmonic and increase of 3.5% in the amplitude of the 5th leads to a reduction in rotor losses and improved torque performance. However, the added complexity of the winding arrangement requires reconsideration of the inductances if the machines is to be controlled in the *dq*-frame.

This work is licensed under a Creative Commons Attribution 4.0 License. For more information, see https://creativecommons.org/licenses/by/4.0/

This article has been accepted for publication in IEEE Access. This is the author's version which has not been fully edited and
content may change prior to final publication. Citation information: DOI 10.1109/ACCESS.2024.3413145

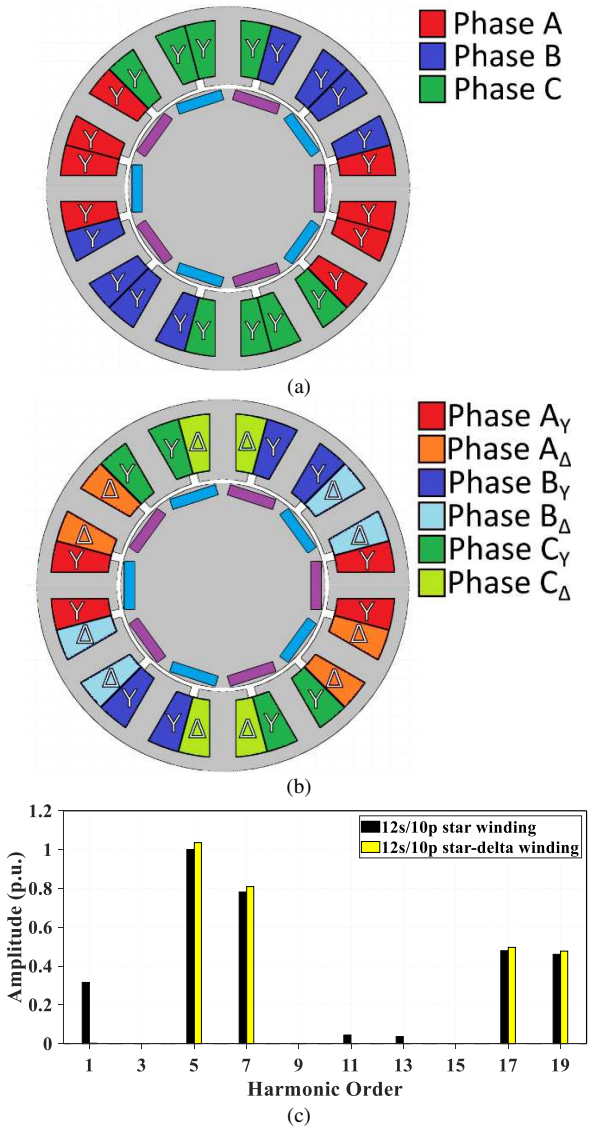

Fig. 3. Comparison of 3-phase 12s/10p machines. (a) Conventional star winding, (b) star-delta winding, and (c) armature MMF harmonics.

TABLE I: SIMULATED MACHINE SPECIFICATIONS

Stator outer radius (mm)	50	Air-gap length (mm)	1
Rotor outer radius (mm)	27.5	Tooth width (mm)	7
Stack length (mm)	50	Tooth tip height (mm)	2.5
Turns/phase - Star	64	Turns/phase - Delta	112
Stator yoke height (mm)	3.7	Magnet thickness (mm)	3
IPM Magnet width (mm)	13	Magnet remanence (T)	1.24

B. Simplified Inductance Model

A simple way to try and obtain the *d*- and *q*-axis inductances of the star-delta wound machine would be to transform the delta inductances to an equivalent 'star' inductance. With an equivalent star winding inductance matrix, the general Park transformation can be applied which would provide approximations for *d*- and *q*-axis inductance. Electrical properties, such as resistance or inductance of the delta-windings, can be transformed to those of an equivalent 'star' winding using Ohm's Law. Inductors in series add up while those in parallel are the reciprocal of the sum of the individual inductance reciprocals. For this method the equivalent star inductances can be calculated from the delta inductances to generate an equivalent inductance model as shown in Fig. 4. For phase A equivalent star inductance, the transformation equation is given by

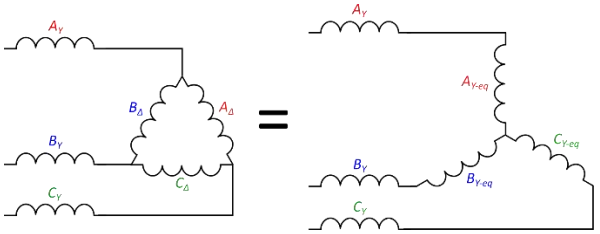

Fig. 4. Circuit simplification after delta to star transformation.

$$L_{aY-eq} = \frac{L_{a\Delta}L_{b\Delta}}{L_{a\Delta} + L_{b\Delta} + L_{c\Delta}} \tag{1}$$

where $L_{a\Delta}$, $L_{b\Delta}$, $L_{c\Delta}$ are the delta coil inductances of phases A, B and C, respectively. Assuming that all delta inductances are equal, and applying the same equation to each phase gives an equivalent star inductance of $L_\Delta/3$. Using this equivalent inductance and assuming a mutual inductance of M_{ph} between phases, the equations for inductance can be derived. In the case of rotor anisotropic magnetic structure, such as the example IPM machine, the self- and mutual inductances are functions of the rotor position. Assuming the geometric and electromagnetic asymmetry of the windings as well as material saturation effects are all negligible, the self-inductance for the 3-phase coils (*i, j = a, b, c* and $i \neq j$) can be expressed as

$$\begin{cases} L_i = L_{Y0} + \dfrac{L_{\Delta 0}}{3} - \left(L_{Y2} + \dfrac{L_{\Delta 2}}{3}\right)\cos 2(\theta_i) \\ M_{ij} = M_{ph0} - M_{ph2}\cos(\theta_i + \theta_j) \end{cases} \tag{2}$$

where L_{Y0} and $L_{\Delta 0}$ denote the average value of star and delta coil self-inductances, respectively. L_{Y2} and $L_{\Delta 2}$ are the second-harmonics (from rotor anisotropy), θ_i and θ_j are the electrical displacement of the *i*th or *j*th winding from the *d*-axis. These equations can then be combined to give a simple 3-phase inductance matrix of the star-delta machine, as described by

$$\boldsymbol{L_{abc}} = \begin{pmatrix} L_A & M_{AB} & M_{AC} \\ M_{BA} & L_B & M_{BC} \\ M_{CA} & M_{CB} & L_C \end{pmatrix} \tag{3}$$

This is a general 3-phase inductance matrix that can be easily transformed to the *dq*-frame using the power-invariant Park transformation given by

$$\boldsymbol{T_p} = \sqrt{\frac{2}{3}}\begin{pmatrix} \cos(\theta) & \cos\left(\theta - \dfrac{2\pi}{3}\right) & \cos\left(\theta + \dfrac{2\pi}{3}\right) \\ -\sin(\theta) & -\sin\left(\theta - \dfrac{2\pi}{3}\right) & -\sin\left(\theta + \dfrac{2\pi}{3}\right) \end{pmatrix} \tag{4}$$

This results in a final *dq*-inductance matrix of

$$\boldsymbol{L_{dq}} = \mathrm{diag}(L_d, L_q) \tag{5}$$

with

$$\begin{cases} L_d = L_{Y0} + \dfrac{L_{\Delta 0}}{3} + M_{ph0} - \dfrac{L_{Y2}}{2} - \dfrac{L_{\Delta 2}}{6} - M_{ph2} \\ L_q = L_{Y0} + \dfrac{L_{\Delta 0}}{3} + M_{ph0} + \dfrac{L_{Y2}}{2} + \dfrac{L_{\Delta 2}}{6} + M_{ph2} \end{cases} \tag{6}$$

It is easy to measure the self-inductance of the individual star and delta coils. However, due to the existence of the delta connection there is no neutral point in a real star-delta machine. Without a neutral point the mutual inductance of phases cannot be measured experimentally. Furthermore, this simple method does not account for the 30° phase shift between currents in the star and delta windings, which could influence the mutual inductance between adjacent coils. To address the shortcomings of the simplified inductance model, a decomposed coil-by-coil model is required to investigate and calculate the mutual inductance between phases as a

This work is licensed under a Creative Commons Attribution 4.0 License. For more information, see https://creativecommons.org/licenses/by/4.0/

This article has been accepted for publication in IEEE Access. This is the author's version which has not been fully edited and
content may change prior to final publication. Citation information: DOI 10.1109/ACCESS.2024.3413145

function of the mutual inductances between each star and delta coil. This will be detailed in the following section.

III. Decomposed Coil-by-Coil Model

To accurately capture the mutual inductance between each coil in the *dq*-model, the voltage equation must be expressed in terms of individual coils as

$$\boldsymbol{u}_{Y\Delta} = \boldsymbol{R}_{Y\Delta}\boldsymbol{i}_{Y\Delta} + j\omega\boldsymbol{\psi}_{Y\Delta} + \boldsymbol{L}_{Y\Delta}\frac{d\boldsymbol{i}_{Y\Delta}}{dt} \tag{7}$$

where the star-delta resistance matrix, current matrix, and total linkages are given by the following.

$$\begin{cases} \boldsymbol{R}_{Y\Delta} = \mathrm{diag}(R_Y, R_\Delta, R_Y, R_\Delta, R_Y, R_\Delta) \\ \boldsymbol{i}_{Y\Delta} = (i_{aY} \quad i_{a\Delta} \quad i_{bY} \quad i_{b\Delta} \quad i_{cY} \quad i_{c\Delta})^T \end{cases} \tag{8}$$

$$\boldsymbol{\psi}_{Y\Delta} = \boldsymbol{L}_{Y\Delta}\boldsymbol{i}_{Y\Delta} + \boldsymbol{\psi}_{\boldsymbol{pm}-Y\Delta} \tag{9}$$

The individual star-delta flux linkages are expressed as a function of the decomposed inductance matrix and individual coil currents, as described by (9), and the PM flux linkage is simply a function of rotor positions and can be expressed as

$$\boldsymbol{\psi}_{\boldsymbol{pm}-Y\Delta} = \psi_{pm}\begin{pmatrix} \cos(\theta) \\ \sqrt{3}\cos(\theta - \pi/6) \\ \cos(\theta - 2\pi/3) \\ \sqrt{3}\cos(\theta - 2\pi/3 - \pi/6) \\ \cos(\theta + 2\pi/3) \\ \sqrt{3}\cos(\theta + 2\pi/3 - \pi/6) \end{pmatrix} \tag{10}$$

where ψ_{pm} is the peak PM flux linkage of a single star phase winding. The shift angles in the PM flux linkage matrix correspond to the electrical space vector of the individual coil, so the delta coils are shifted by 30 elec. deg. with respect to the star coils. The $\sqrt{3}$ accounts for the number of turns in the delta coils and is directly proportional to flux linkage. To calculate the total star-delta flux linkage in (9) the inductance matrix must be derived as a function of rotor position.

A. Decomposed Stator Inductance Matrix

For the decomposed inductance matrix, the equation for self-inductance (2) is split into two equations, one for star coil self-inductance and one for delta coil self-inductance ($i = a, b, c$)

$$\begin{cases} L_{iY} = L_{Y0} - L_{Y2}\cos 2(\theta_i) \\ L_{i\Delta} = L_{\Delta 0} - L_{\Delta 2}\cos 2(\theta_i - \pi/6) \end{cases} \tag{11}$$

To generate equations for mutual inductance, the coils must firstly be decomposed into star-star pairs and delta-delta pairs for each phase ($i, j = a, b, c$ and $i \neq j$). As before, these mutual inductances are comprised of a fundamental component (M_{YY0}, $M_{\Delta\Delta 0}$) and a 2nd harmonic component (M_{YY2}, $M_{\Delta\Delta 2}$), as described by

$$\begin{cases} M_{iYjY} = M_{YY0} - M_{Y2}\cos(\theta_i + \theta_j) \\ M_{i\Delta j\Delta} = M_{\Delta\Delta 0} - M_{\Delta 2}\cos(\theta_i + \theta_j - \pi/6) \end{cases} \tag{12}$$

These equations are not dissimilar from a conventional 3-phase winding when operating in isolation, albeit the delta coils are shifted by $\pi/6$ (or 30) elec. deg. from the *d*-axis. For the star-delta winding there exists cross-coupling between star and delta coils of each phase group which again is a function of rotor position. Furthermore, as can be seen in Fig. 3(a) each star coil is adjacent to two delta coils, and each delta coil is adjacent to two star coils. This results in a different equation for mutual inductance depending on which star-delta coils are paired. As inductance is inversely proportional to the air-gap length, it can be assumed that the second harmonic of the mutual inductance is inversely proportional to the number of slot pitches, *sp*, between star-delta coil pairs. Therefore, the mutual inductance for star-delta coil pairs for each phase ($i, j = a, b, c$) can be expressed as

$$M_{iYj\Delta} = M_{Y\Delta 0}\cos(\theta_i + \theta_j - \pi/6) - \frac{1}{sp}M_{Y\Delta 2}\cos(\gamma_{ij}) \tag{13}$$

with

$$\gamma_{ij} = \begin{cases} 2(\theta_i - \pi/12) & \text{if } ij = a_Y a_\Delta, b_Y b_\Delta, c_Y c_\Delta \\ 2(\theta_i - 5\pi/12) & \text{if } ij = a_Y b_\Delta, b_Y c_\Delta, c_Y a_\Delta \\ 2(\theta_i + \pi/4) & \text{if } ij = a_Y c_\Delta, b_Y a_\Delta, c_Y b_\Delta \end{cases} \tag{14}$$

where *sp* is the number of slots between the star-delta coil pair. Combining these equations together into a 6x6 matrix of decomposed coil self- and mutual inductances gives the final $\boldsymbol{L}_{Y\Delta}$ matrix below.

$$\boldsymbol{LY\Delta} = \begin{bmatrix} L_{aY} & M_{aYa\Delta} & M_{aYbY} & M_{aYb\Delta} & M_{aYcY} & M_{aYc\Delta} \\ M_{aYa\Delta} & L_{a\Delta} & M_{bYa\Delta} & M_{a\Delta b\Delta} & M_{cYa\Delta} & M_{a\Delta c\Delta} \\ M_{bYaY} & M_{bYa\Delta} & L_{bY} & M_{bYb\Delta} & M_{bYcY} & M_{bYc\Delta} \\ M_{aYb\Delta} & M_{b\Delta a\Delta} & M_{bYb\Delta} & L_{b\Delta} & M_{cYb\Delta} & M_{b\Delta c\Delta} \\ M_{cYaY} & M_{cYa\Delta} & M_{cYbY} & M_{cYb\Delta} & L_{cY} & M_{cYc\Delta} \\ M_{aYc\Delta} & M_{c\Delta a\Delta} & M_{bYc\Delta} & M_{c\Delta b\Delta} & M_{cYc\Delta} & L_{c\Delta} \end{bmatrix} \tag{15}$$

To validate these equations, an FEA model was built for the 12s/10p IPM machine investigated. Each coil was excited by a current of 1A and the self- and mutual inductances calculated for each case. The average values and 2nd harmonic components were then used in the above matrix to generate analytical waveforms of inductance for comparison with the FEA results. Fig. 5(a) shows the self-inductance of coil A_Y as well as the mutual inductances with its adjacent delta coils A_Δ and B_Δ. Fig. 5(b) shows the mutual inductance of coil A_Y with the non-adjacent coils B_Y, C_Y, and C_Δ.

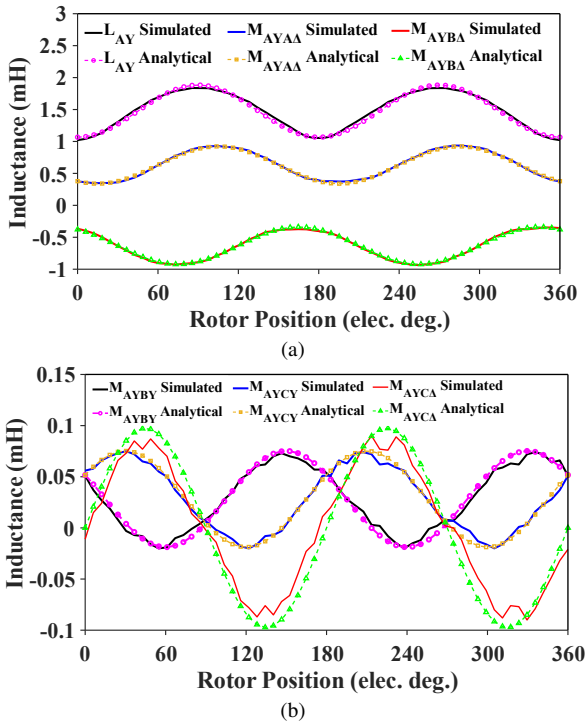

Fig. 5. Comparison of analytical inductances and FEA obtained. (a) Self-inductance and adjacent coil mutual inductance and (b) non-adjacent coil mutual inductance.

This work is licensed under a Creative Commons Attribution 4.0 License. For more information, see https://creativecommons.org/licenses/by/4.0/

This article has been accepted for publication in IEEE Access. This is the author's version which has not been fully edited and content may change prior to final publication. Citation information: DOI 10.1109/ACCESS.2024.3413145

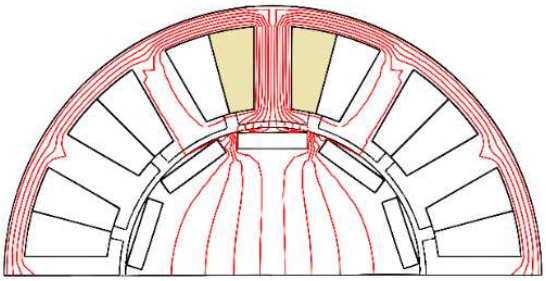

Fig. 6. Flux lines produced by coil A_Y supplied by a 1A DC current.

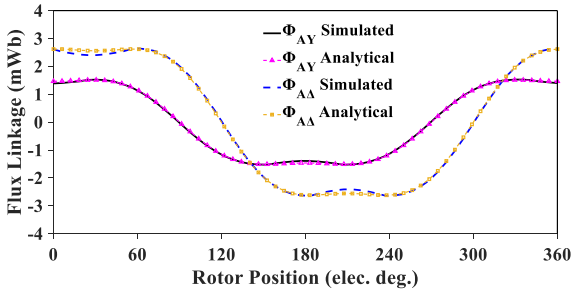

Fig. 7. Armature flux linkage comparison of simulated and analytical results using simplified inductance matrix.

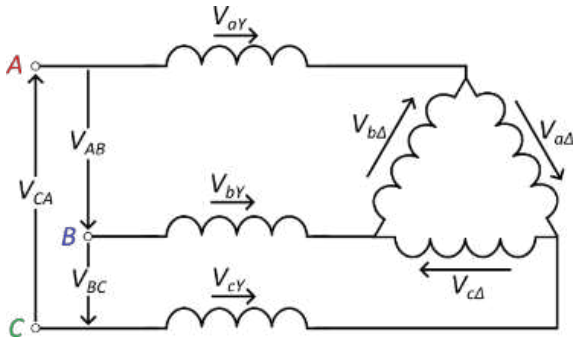

Fig. 8. Line Voltage summation.

It can be seen in Fig. 5 that the mutual inductances between non-adjacent coils is very small and so can be neglected. This can be validated with FEA by plotting the flux lines produced by coil A_Y supplied with a 1A DC current, as displayed in Fig. 6. These flux lines only cross through the adjacent coils A_Δ and B_Δ, thus it can be reasonably concluded that mutual inductance only needs to be considered for adjacent coils. This produces a simplified inductance matrix with only adjacent coil mutual inductances $\boldsymbol{L_{Y\Delta}}$.

$$\boldsymbol{LY\Delta} = \begin{bmatrix} L_{aY} & M_{aYa\Delta} & 0 & M_{aYb\Delta} & 0 & 0 \\ M_{aYa\Delta} & L_{a\Delta} & 0 & 0 & M_{cYa\Delta} & 0 \\ 0 & 0 & L_{bY} & M_{bYb\Delta} & 0 & M_{bYc\Delta} \\ M_{aYb\Delta} & 0 & M_{bYb\Delta} & L_{b\Delta} & 0 & 0 \\ 0 & M_{cYa\Delta} & 0 & 0 & L_{cY} & M_{cYc\Delta} \\ 0 & 0 & M_{bYc\Delta} & 0 & M_{cYc\Delta} & L_{c\Delta} \end{bmatrix} \tag{16}$$

For further verification, the FEA model was used to generate flux linkages for comparison with the results obtained from the simplified inductance matrix. After aligning the *d*-axis with coil A_Y, the machine was spun first under open-circuit condition and then supplied with 1A *d*-axis current. The resulting flux linkage for coils A_Y and A_Δ generated due to armature windings only was then calculated using

$$\psi_{coil} = \psi_{total} - \psi_{pm} \tag{17}$$

where ψ_{total} is the flux linkage produced by both PMs and *d*-axis current and ψ_{pm} is the open-circuit flux linkage. The results were then compared with calculated analytical armature flux linkage using the simplified inductance matrix (16) and the decomposed star-delta current matrix in (8) and can be seen in Fig. 7. There is a very close match between the FEA results and the analytical results obtained using the simplified inductance matrix. Therefore, it is safe to ignore the mutual inductance of non-adjacent coils when translating to the *dq*-frame.

IV. ABC TO DQ TRANSFORMATION

To transform the star-delta voltage equation (7) to the *dq*-frame, it must first be translated from its YΔ-form to the *abc*-frame. As there is no neutral point, the individual coil voltages and flux linkages must first be summed to give line properties using a matrix $\boldsymbol{A}$. For *dq*-analysis, the star-delta currents must be expressed as a function of the *abc*-currents using a matrix $\boldsymbol{B}$. The *abc*-currents can then be transformed into the *dq*-frame using the Park and inverse Park Transform. This gives an equation for the line voltage of the form

$$\boldsymbol{u_{line}} = \boldsymbol{AR_{Y\Delta}BT_p^T i_{dq}} + j\omega\boldsymbol{A\psi_{Y\Delta}} + \boldsymbol{AL_{Y\Delta}BT_p^T}\frac{d\boldsymbol{i_{dq}}}{dt} \tag{18}$$

Applying the same logic to the star-delta flux linkages in (9) gives an expression for line flux linkage as

$$\boldsymbol{\psi_{line}} = \boldsymbol{AL_{Y\Delta}BT_p^T i_{dq}} + \boldsymbol{A\psi_{pm-Y\Delta}} \tag{19}$$

To express the *dq*-inductance in terms of the decomposed star-delta coil inductances the matrices $\boldsymbol{A}$ and $\boldsymbol{B}$ must be obtained.

A. Voltage Transformation Matrix (A)

The line voltages and flux linkage can be obtained by taking the phasor sum of the individual coil voltages or flux linkage between two points. For example, the line voltage between A and B (V_{AB}) is the sum of individual coil voltages V_{aY}, $V_{b\Delta}$, and V_{bY}. As the voltages V_{bY} and $V_{b\Delta}$ are shifted by 120 and 150 elec. deg. from V_{aY} respectively they are multiplied by -1 in the transformation matrix. The full circuit diagram showing how the line voltages are obtained from individual coil voltages can be seen in Fig. 8. The same process can be applied for flux linkage to give the same matrix. This gives the voltage transformation matrix $\boldsymbol{A}$ as

$$\boldsymbol{A} = \begin{bmatrix} 1 & 0 & -1 & -1 & 0 & 0 \\ 0 & 0 & 1 & 0 & -1 & 1 \\ -1 & -1 & 0 & 0 & 1 & 0 \end{bmatrix} \tag{20}$$

B. Current Transformation Matrix (B)

To transform the star-delta voltages to the *dq*-frame, the individual coil currents must be expressed as a function of the supply (or star coil) currents. As the delta currents are all reduced by a magnitude of $\sqrt{3}$ and shifted by 30° with respect to the star currents, there should exist a circular matrix that can perform this transformation. This can be expressed in the form

$$\boldsymbol{i_\Delta} = \begin{bmatrix} x & y & z \\ z & x & y \\ y & z & x \end{bmatrix} i_Y \tag{21}$$

By simply equating the left side of the equation with the right gives equation (22) for obtaining the delta currents as functions of the star currents with three unknowns *x*, *y*, and *z*. Using trigonometric identities, it is possible to expand these equations to provide a simplified set of equations that can be used to obtain the unknown variables, $x = 1/2$, $y = 1/6$ and $z =$

This work is licensed under a Creative Commons Attribution 4.0 License. For more information, see https://creativecommons.org/licenses/by/4.0/

This article has been accepted for publication in IEEE Access. This is the author's version which has not been fully edited and content may change prior to final publication. Citation information: DOI 10.1109/ACCESS.2024.3413145

$$\begin{cases} i_{a\Delta} = \frac{1}{\sqrt{3}}\cos\left(\theta - \frac{\pi}{6}\right) = x\cos(\theta) + y\cos\left(\theta - \frac{2\pi}{3}\right) + z\cos\left(\theta + \frac{2\pi}{3}\right) \\ i_{b\Delta} = \frac{1}{\sqrt{3}}\cos\left(\theta - \frac{2\pi}{3} - \frac{\pi}{6}\right) = z\cos(\theta) + x\cos\left(\theta - \frac{2\pi}{3}\right) + y\cos\left(\theta + \frac{2\pi}{3}\right) \\ i_{c\Delta} = \frac{1}{\sqrt{3}}\cos\left(\theta + \frac{2\pi}{3} - \frac{\pi}{6}\right) = y\cos(\theta) + z\cos\left(\theta - \frac{2\pi}{3}\right) + x\cos\left(\theta + \frac{2\pi}{3}\right) \end{cases} \quad (22)$$

-1/6. Combining these values into the identity matrix gives a circular matrix $\boldsymbol{B}$ that can decompose the supply *abc*-frame currents into individual star and delta coil currents.

$$\boldsymbol{B} = \begin{bmatrix} 1 & 0 & 0 \\ 1/2 & 1/6 & -1/6 \\ 0 & 1 & 0 \\ -1/6 & 1/2 & 1/6 \\ 0 & 0 & 1 \\ 1/6 & -1/6 & 1/2 \end{bmatrix} \begin{matrix} \leftarrow i_{aY} \\ \leftarrow i_{a\Delta} \\ \leftarrow i_{bY} \\ \leftarrow i_{b\Delta} \\ \leftarrow i_{cY} \\ \leftarrow i_{c\Delta} \end{matrix} \quad (23)$$

C. Line Flux-Linkage to dq-Frame

To transform voltages from *abc*-frame to *dq*-frame the power-invariant Park transformation (4) is used. However, the Park transform is for use with phase voltages and flux linkages. Therefore, the line flux linkage must be expressed in terms of phase flux linkage before transforming to the *dq*-frame. For this, (19) is first expressed as a function of phase flux linkage as described by

$$\boldsymbol{\psi_{line}} = \begin{pmatrix} \psi_{a0} - \psi_{b0} \\ \psi_{b0} - \psi_{c0} \\ \psi_{c0} - \psi_{a0} \end{pmatrix} = \begin{pmatrix} \psi_{a0} \\ \psi_{b0} \\ \psi_{c0} \end{pmatrix} - \begin{pmatrix} 0 & 1 & 0 \\ 0 & 0 & 1 \\ 1 & 0 & 0 \end{pmatrix} \begin{pmatrix} \psi_{a0} \\ \psi_{b0} \\ \psi_{c0} \end{pmatrix} \quad (24)$$

With the phase flux linkage separated, the Park and inverse Park transformations can be applied to obtain the *dq*-axis flux linkages. These can then be summed and inversed to give an expression for *dq*-frame flux linkages as a function of the *abc* line flux linkages, as demonstrated in equations (25a-d).

$$\boldsymbol{T_p\psi_{line}} = \boldsymbol{T_p}\begin{pmatrix} \psi_{a0} \\ \psi_{b0} \\ \psi_{c0} \end{pmatrix} - \boldsymbol{T_p}\begin{pmatrix} 0 & 1 & 0 \\ 0 & 0 & 1 \\ 1 & 0 & 0 \end{pmatrix}\boldsymbol{T_p^T T_p}\begin{pmatrix} \psi_{a0} \\ \psi_{b0} \\ \psi_{c0} \end{pmatrix} \quad (25a)$$

$$\boldsymbol{T_p\psi_{line}} = \boldsymbol{\psi_{dq}} - \frac{1}{2}\begin{pmatrix} -1 & \sqrt{3} \\ -\sqrt{3} & -1 \end{pmatrix}\boldsymbol{\psi_{dq}} \quad (25b)$$

$$\boldsymbol{T_p\psi_{line}} = \frac{\sqrt{3}}{2}\begin{pmatrix} \sqrt{3} & -1 \\ 1 & \sqrt{3} \end{pmatrix}\boldsymbol{\psi_{dq}} \quad (25c)$$

$$\boldsymbol{\psi_{dq}} = \frac{1}{2\sqrt{3}}\begin{pmatrix} \sqrt{3} & 1 \\ -1 & \sqrt{3} \end{pmatrix}\boldsymbol{T_p\psi_{line}} \quad (25d)$$

Applying this transformation together with the matrices $\boldsymbol{A}$ and $\boldsymbol{B}$, an expression for *dq*-frame flux linkages can be obtained, which is based on the decomposed stator inductance matrix and matrix $\boldsymbol{C}$.

$$\boldsymbol{\psi_{dq}} = \boldsymbol{CT_pAL_{Y\Delta}BT_p^T i_{dq}} + \boldsymbol{CT_pA\psi_{pm-Y\Delta}} \quad (26)$$

with

$$\boldsymbol{C} = \frac{1}{2\sqrt{3}}\begin{pmatrix} \sqrt{3} & 1 \\ -1 & \sqrt{3} \end{pmatrix} \quad (27)$$

Finally, this can be used to obtain the *d*- and *q*-axis inductances and PM flux linkages such as

$$\boldsymbol{L_{dq}} = \begin{pmatrix} L_d & 0 \\ 0 & L_q \end{pmatrix} = \boldsymbol{CT_pAL_{Y\Delta}BT_p^T} \quad (28)$$

$$\boldsymbol{\psi_{dq-pm}} = \boldsymbol{CT_pA\psi_{pm-Y\Delta}} = \begin{pmatrix} \sqrt{6}\psi_{pm} \\ 0 \end{pmatrix} \quad (29)$$

with

$$\begin{cases} L_d = L_{Y0} + \frac{L_{\Delta 0}}{3} + 2M_{Y\Delta 0} - \frac{L_{Y2}}{2} - \frac{L_{\Delta 2}}{6} - \frac{2M_{Y\Delta 2}}{\sqrt{3}} \\ L_q = L_{Y0} + \frac{L_{\Delta 0}}{3} + 2M_{Y\Delta 0} + \frac{L_{Y2}}{2} + \frac{L_{\Delta 2}}{6} + \frac{2M_{Y\Delta 2}}{\sqrt{3}} \end{cases} \quad (30)$$

The fundamental components of *d*- and *q*- axis inductances are the same as in (6), with M_{ph0} being equal to $2M_{Y\Delta 0}$. The 2nd harmonic components of the star-delta coil mutual inductance M_{ph2} has been found to equal $2M_{Y\Delta 2}/\sqrt{3}$. Therefore, it has been demonstrated that to obtain the *d*- and *q*-axis inductances of a star-delta machine, the inductances of individual star and delta coils must be measured in addition to the mutual inductance of an adjacent star-delta coil pair. Comparing these equations with what would be expected for a conventional 3-phase machine, the 2nd harmonic of mutual inductance is multiplied by a factor of $2/\sqrt{3}$ (or 1.15). As this value is subtracted to the *d*-axis inductance and added to the *q*-axis inductance, it is expected that this winding topology will improve the difference between *d*- and *q*-axis inductances. Applying the same process to the resistance matrix given in (8), the *dq*-frame resistances can be obtained.

$$\boldsymbol{R_{dq}} = \boldsymbol{CT_pAR_{Y\Delta}BT_p^T} \quad (31)$$

$$\boldsymbol{R_{dq}} = \mathrm{diag}(R_Y + \frac{R_\Delta}{3}, R_Y + \frac{R_\Delta}{3}) \quad (32)$$

The *dq*-voltage equation can be obtained by applying the same process to the differential current term in (18), resulting in (33) that can be used for *dq*-analysis of star-delta wound machines.

$$\boldsymbol{u_{dq}} = \boldsymbol{R_{dq}i_{dq}} + j\omega\boldsymbol{\psi_{dq}} + \boldsymbol{L_{dq}}\frac{d\boldsymbol{i_{dq}}}{dt} \quad (33)$$

D. Comparison with Conventional Winding Connection

Both the star-delta connected IPM and SPM machines specified in TABLE I were modelled in FEA and compared with an identical machine with star connected windings. The Park and inverse Park transformations were applied to the 3-phase machines with conventional winding connection to obtain *d*- and *q*-axis inductances, and (28) was used to obtain the *d*- and *q*-axis inductances for the star-delta wound machines. The results are plotted for one electrical period in Fig. 9 and inductances directly compared in TABLE II.

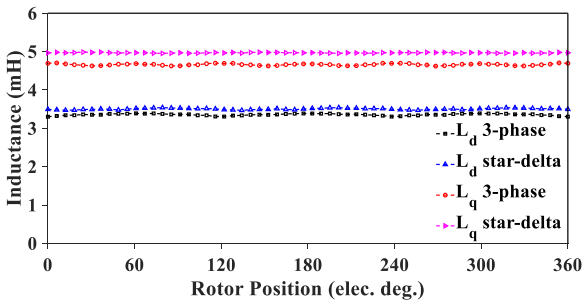

(a)

This work is licensed under a Creative Commons Attribution 4.0 License. For more information, see https://creativecommons.org/licenses/by/4.0/

This article has been accepted for publication in IEEE Access. This is the author's version which has not been fully edited and
content may change prior to final publication. Citation information: DOI 10.1109/ACCESS.2024.3413145

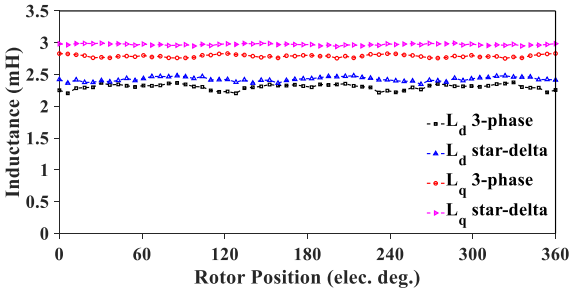

(b)

Fig. 9. *dq*-frame inductance comparison between 3-phase star winding and star-delta winding. (a) IPM, and (b) SPM.

TABLE II *DQ*-FRAME INDUCTANCE COMPARISON

	L_d (mH)	L_q (mH)	L_q/L_d
3-phase IPM	3.366	4.662	1.389
Star-delta IPM	3.505	4.969	1.418
3-phase SPM	2.304	2.790	1.211
Star-delta SPM	2.426	2.9719	1.225

For both the IPM and SPM machines, their *d*- and *q*-axis inductances are slightly increased by employing a hybrid star-delta winding. Furthermore, the harmonic elimination property of the star-delta winding appears to reduce the ripple within the *dq*-inductance waveforms. This could lead to reduced reluctance torque ripple of the IPM machine. Finally, for both the IPM and SPM machines the saliency ratio of the inductances has been increased. For the IPM machine the increase is 2.1% and for the SPM machine it is 1.2%. Although these are not incredibly large values, they could increase the reluctance torque capability for the IPM machine and sensorless control capability of the SPM machine.

V. Experimental Validation

A. Experimental Setup

A dual 3-phase 24s/10p machine with two sets of star-delta windings was manufactured for experimental validation of the inductance calculations and transformations. This prototype has a coil pitch of 2 and so the inductances will not exactly match those in Section III. However, each of the two 3-phase winding sets is identical to the layout of Fig. 3 (b). The *dq*-transformation proposed relies only on the winding structure and is independent of slot-pole number or coil pitch. Therefore, with only one winding set studied, this experimental validation will still demonstrate the applicability of this method. Additionally minor modification was made to the IPM rotor that was investigated experimentally. Any updates to the dimensions of the machine are given in TABLE III, with all other properties remaining the same as given in TABLE I. The star-delta winding layout, IPM rotor, and test setup can be seen in Fig. 10.

B. Impact of Coil Location

As highlighted previously, the number of turns in the delta coils is $\sqrt{3}$ times the number of turns in the star coil. As inductance is proportional to the square of coil turns, it was expected that the delta coil inductance would be 3 times larger than the star coil inductance. During the investigation, it was found to be only approximately 2.5 times larger. This has been found to be attributed to the location of the coils within the stator slots. As evident in Fig. 10, the double-layer winding has been constructed with coils placed radially within the slots, and specifically all star coils were wound first and placed at the slot bottom. This meant that all delta

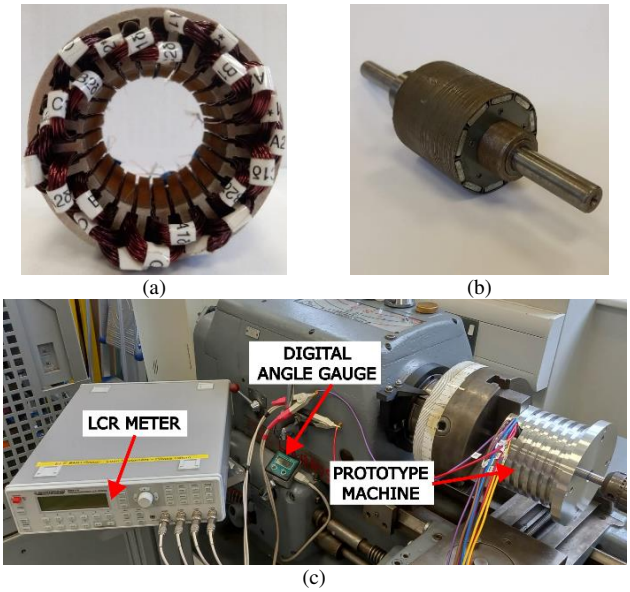

(a) (b) (c)

Fig. 10. 24s/10p star-delta wound prototype machine. (a) Stator with winding layout, (b) 10-pole IPM rotor, and (c) experimental setup.

TABLE III PROTOTYPE MACHINE MODIFICATIONS

Turns/phase - Star	32	IPM air-gap length (mm)	2.5
Turns/phase - Delta	56	IPM rotor outer radius (mm)	26
Tooth width (mm)	3.5	IPM magnet width (mm)	14

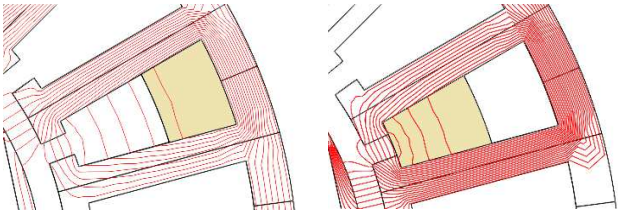

(a) (b)

Fig. 11. Flux lines showing slot leakage under 1A excitation for (a) star coil, and (b) delta coil.

coils were wound towards the top of the slot, and so are more subject to slot leakage thus reducing their self-inductance. This has been validated using FEA by investigating the slot leakage of a star and delta coil respectively, as shown in Fig. 11. Here, 1A dc is supplied and the PMs have been removed.

C. *DQ*-frame *Inductances*

The individual star and delta coil inductances, as well as mutual inductances, were measured while rotating the machine through one electrical period to obtain rotor position-based inductances. These were then compared against simulated results and are plotted in Fig. 12 (a) and Fig. 13 (a) for the IPM and SPM machines respectively. The inductance matrix in (16) was then composed using each simulated and measured inductance waveform, and using (28), the *d*- and *q*-axis inductances can also be compared, as shown in Fig. 12 (b) and Fig. 13 (b). It can be seen in both cases that the measured inductances are slightly higher than the simulated ones. This is due to the end-winding inductance that is present in the real machine but not accounted for in 2D simulation. However, this difference is generally very small, so a more time-consuming 3D simulation is deemed unnecessary.

For a direct comparison of the simulated and measured results, two methods were used to obtain the *d*- and *q*-axis inductances. Method 1 uses the simulated and measured self-inductances for coils A_Y and A_Δ, as well as their mutual inductance. These values are then used with (30) to calculate the *d*- and *q*-axis inductances. Method 2 uses the complete

This work is licensed under a Creative Commons Attribution 4.0 License. For more information, see https://creativecommons.org/licenses/by/4.0/

This article has been accepted for publication in IEEE Access. This is the author's version which has not been fully edited and
content may change prior to final publication. Citation information: DOI 10.1109/ACCESS.2024.3413145

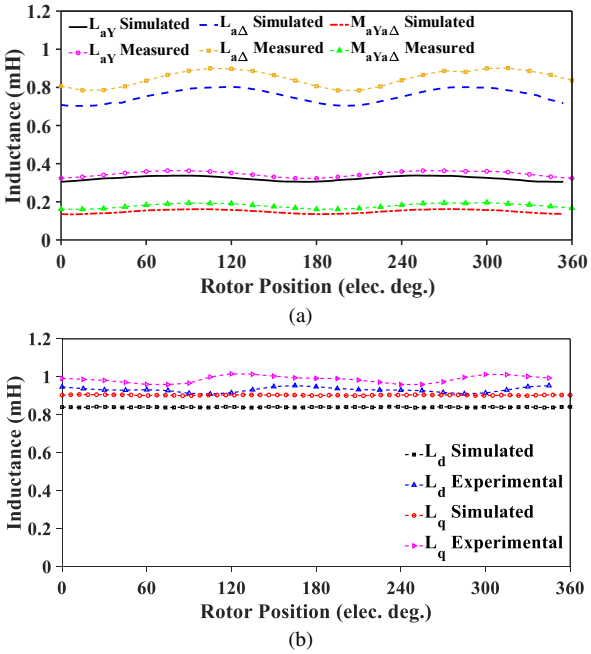

Fig. 12. IPM rotor inductance comparison. (a) Star and delta coil inductances and adjacent coil mutual inductance, and (b) *d*- and *q*-axis inductances.

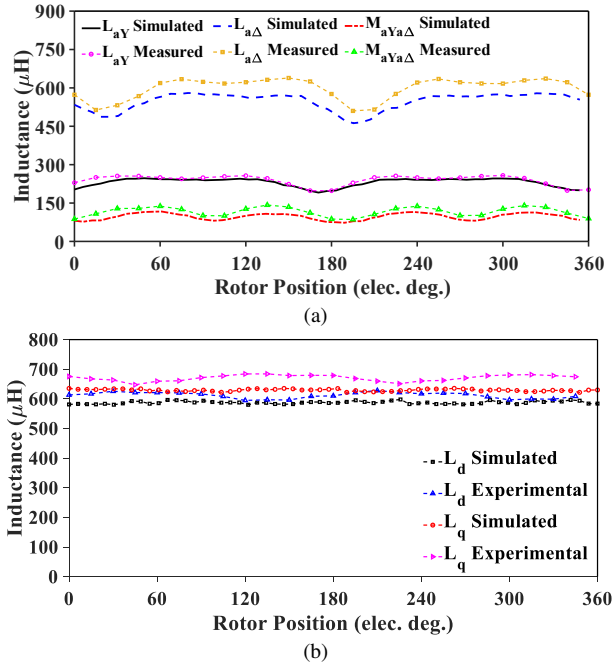

Fig. 13. SPM rotor inductance comparison. (a) Star and delta coil inductances and adjacent coil mutual inductance, and (b) *d*- and *q*-axis inductances.

TABLE IV SIMULATED AND MEASURED L_d AND L_q (μH)

		L_d simulated	L_d measured	L_q simulated	L_q measured
IPM	Method 1	838.61	942.94	903.94	1023.8
	Method 2	840.38	931.87	903.85	987.37
SPM	Method 1	557.42	610.62	655.89	727.83
	Method 2	587.54	611.96	629.44	670.67

transformation (28) after obtaining all coil inductances and mutual inductances. The average value of *d*- and *q*-axis inductance is then calculated over one electrical period. The comparison of the results for these two methods can be seen in TABLE IV for both the IPM machine and SPM machine. It is also found that the measured inductances are about 10% larger than the simulated inductances for both machines. Again, this is expected due to the end-winding inductance presented in the real machine. However, there is very good agreement between Method 1 for *d*- and *q*-axis inductance calculation and calculating the inductances with Method 2, validating equation (30). Thus, demonstrating that the *d*- and *q*-axis inductances for a star-delta wound FSCW machine can be obtained using only the self-inductances of an individual star and delta coil, as well as their mutual inductance.

VI. Conclusion

In this paper a method for transformation of *abc*-reference frame parameters in star-delta wound synchronous machines to the *dq*-reference frame is presented. This allows for *dq*-analysis of such machines. The proposed method uses a decomposed coil-by-coil inductance matrix that accounts for the dependence of inductance on rotor position as well as phase shift of currents between the two series connected star and delta coils. This transformation solves the problem of there being no neutral point in a hybrid star-delta wound machine, which prevents measurement of the phase mutual inductances. This work demonstrates that the *d*- and *q*-axis inductances can instead be calculated using only coil self-inductance and the mutual inductance between an adjacent star-delta coil pair.

This method has been first applied to an IPM machine with rotor anisotropy and analytical equations used in the matrices are corroborated by FEA simulations. Both an IPM and SPM machine are then investigated, and it is found that the star-delta winding structure can increase the saliency ratio of both machine types. Thus, enhancing the reluctance torque and sensorless control capability of these FSCW machines. The work is then further validated experimentally using a 24s/10p 3-phase star-delta wound machine. It is found that the calculated inductances closely match that of the prototype. Both simulated and measured inductances are transformed to the *dq*-frame, and it is proven that the *d*- and *q*-axis inductances for a star-delta wound machine can be obtained by only measuring the self- and mutual inductances of an adjacent star-delta coil pair.

Acknowledgement

This work is supported by the UK EPSRC Prosperity Partnership “A New Partnership in Offshore Wind” under Grant No. EP/R004900/1.

For the purpose of open access, the author has applied a Creative Commons Attribution (CC BY) licence to any Author Accepted Manuscript version arising.

VII. References

[1] A. M. El-Refaie, "Fractional-slot concentrated-windings synchronous permanent magnet machines: Opportunities and challenges," *IEEE Trans. Ind. Electron.,* vol. 57, no. 1, pp. 107-121, Jan. 2010.

[2] N. Bianchi, S. Bolognani, M. D. Pre, and G. Grezzani, "Design considerations for fractional-slot winding configurations of synchronous machines," *IEEE Trans. Ind Appl,* vol. 42, no. 4, pp. 997-1006, July 2006.

[3] D. Ishak, Z. Q. Zhu, and D. Howe, "Comparative study of permanent magnet brushless motors with all teeth and alternative teeth windings," presented at the Second IEE International Conference on Power Electronics, Machines and Drives, Edinburgh, UK, Mar., 2004.

[4] K. Atallah, D. Howe, P. H. Mellor, and D. A. Stone, "Rotor loss in permanent magnet brushless ac machines," in *IEEE International Electric Machines and Drives Conference. IEMDC'99. Proceedings*, 1999: IEEE.

[5] N. Bianchi and E. Fornasiero, "Impact of mmf space harmonic on rotor losses in fractional-slot permanent-magnet machines," *IEEE Trans. Energy Convers.,* vol. 24, no. 2, pp. 323-328, June 2009.

This work is licensed under a Creative Commons Attribution 4.0 License. For more information, see https://creativecommons.org/licenses/by/4.0/

This article has been accepted for publication in IEEE Access. This is the author's version which has not been fully edited and
content may change prior to final publication. Citation information: DOI 10.1109/ACCESS.2024.3413145

[6] M. Nakano, H. Kometani, and M. Kawamura, "A study on eddy-current losses in rotors of surface permanent-magnet synchronous machines," *IEEE Trans. Ind Appl,* vol. 42, no. 2, pp. 429-435, Mar. 2006.
[7] P. B. Reddy, A. M. El-Refaie, and K.-K. Huh, "Effect of number of layers on performance of fractional-slot concentrated-windings interior permanent magnet machines," in *8th International Conference on Power Electronics - ECCE Asia*, May 2011: IEEE.
[8] P. B. Reddy, K.-K. Huh, and A. M. El-Refaie, "Generalized approach of stator shifting in interior permanent-magnet machines equipped with fractional-slot concentrated windings," *IEEE Trans. Ind. Electron.,* vol. 61, no. 9, pp. 5035-5046, Sept. 2014.
[9] A. M. El-Refaie, M. R. Shah, R. Qu, and J. M. Kern, "Effect of number of phases on losses in conducting sleeves of surface pm machine rotors equipped with fractional-slot concentrated windings," *IEEE Trans. Ind Appl,* vol. 44, no. 5, pp. 1522-1532, Sept. 2008.
[10] A. S. Abdel-Khalik, S. Ahmed, and A. M. Massoud, "A six-phase 24-slot/10-pole permanent-magnet machine with low space harmonics for electric vehicle applications," *IEEE Trans. Magn.,* vol. 52, no. 6, pp. 1-10, June 2016.
[11] A. S. Abdel-Khalik, S. Ahmed, and A. M. Massoud, "Low space harmonics cancelation in double-layer fractional slot winding using dual multiphase winding," *IEEE Trans. Magn.,* vol. 51, no. 5, pp. 1-10, May 2015.
[12] O. Misir, S. M. Raziee, N. Hammouche, C. Klaus, R. Kluge, and B. Ponick, "Prediction of losses and efficiency for three-phase induction machines equipped with combined star–delta windings," *IEEE Trans. Ind Appl,* vol. 53, no. 4, July 2017.
[13] S. M. Raziee, O. Misir, and B. Ponick, "Combined star-delta winding analysis," *IEEE Trans. Energy Convers.,* vol. 33, no. 1, Mar. 2018.
[14] S. M. Raziee, O. Misir, and B. Ponick, "Multiple multiphase combined star–polygon winding analysis," *IEEE Trans. Ind. Electron.,* vol. 66, no. 10, Oct. 2019.
[15] W. Zhao, J. Zheng, J. Ji, S. Zhu, and M. Kang, "Star and delta hybrid connection of a fscw pm machine for low space harmonics," *IEEE Trans. Ind. Electron.,* vol. 65, no. 12, pp. 9266-9279, Dec. 2018.
[16] A. S. Abdel-Khalik, S. Ahmed, and A. M. Massoud, "Effect of multilayer windings with different stator winding connections on interior pm machines for ev applications," *IEEE Trans. Magn.,* vol. 52, no. 2, pp. 1-7, Feb. 2016.
[17] M. N. Ibrahim, P. Sergeant, and E. E. M. Rashad, "Combined star-delta windings to improve synchronous reluctance motor performance," *IEEE Trans. Energy Convers.,* vol. 31, no. 4, Dec. 2016.
[18] S. Baka, S. Sampathirao, and B. G. Fernandes, "Influence of zero-sequence circulating current on the performance of star-delta winding line-start ferrite assisted synchronous reluctance motor.," *IEEE Trans. Energy Convers.,* pp. 1-1, Jan. 2022.
[19] R. H. Park, "Two-reaction theory of synchronous machines generalized method of analysis-part i," *Transactions of the American Institute of Electrical Engineers,* vol. 48, no. 3, pp. 716-727, July 1929.
[20] R. Gabriel, W. Leonhard, and C. J. Nordby, "Field-oriented control of a standard ac motor using microprocessors," *IEEE Trans. Ind Appl,* vol. IA-16, no. 2, pp. 186-192, Mar. 1980.
[21] R. Wu and G. R. Slemon, "A permanent magnet motor drive without a shaft sensor," *IEEE Trans. Ind Appl,* vol. 27, no. 5, pp. 1005-1011, Jan. 1991.
[22] Z. Chen, M. Tomita, S. Doki, and S. Okuma, "An extended electromotive force model for sensorless control of interior permanent-magnet synchronous motors," *IEEE Trans. Ind. Electron.,* vol. 50, no. 2, pp. 288-295, Apr. 2003.
[23] Z. Zhu, S. Wang, B. Shao, L. Yan, P. Xu, and Y. Ren, "Advances in dual-three-phase permanent magnet synchronous machines and control techniques," *Energies,* vol. 14, no. 22, p. 7508, Nov. 2021.
[24] E. Fuchs and L. Rosenberg, "Analysis of an alternator with two displaced stator windings," *IEEE Trans. Power App. Syst.,* vol. PAS-93, no. 6, Nov. 1974.
[25] R. Schiferl and C. Ong, "Six phase synchronous machine with ac and dc stator connections, part i: Equivalent circuit representation and steady-state analysis," *IEEE Trans. Power App. Syst.,* vol. PAS-102, no. 8, Aug. 1983.
[26] Y. Zhao and T. A. Lipo, "Space vector pwm control of dual three-phase induction machine using vector space decomposition," *IEEE Trans. Ind Appl,* vol. 31, no. 5, Jan. 1995.
[27] Y. Hu, Z. Q. Zhu, and M. Odavic, "Comparison of two-individual current control and vector space decomposition control for dual three-phase pmsm," *IEEE Trans. Ind Appl,* vol. 53, no. 5, Sept. 2017.
[28] H. Knudsen, "Extended park's transformation for 2×3-phase synchronous machine and converter phasor model with representation of ac harmonics," *IEEE Trans. Energy Convers.,* vol. 10, no. 1, Mar. 1995.
[29] M. Andriollo, G. Bettanini, G. Martinelli, A. Morini, and A. Tortella, "Analysis of double star permanent magnet synchronous generators by a general decoupled d-q model," in *2007 IEEE International Electric Machines & Drives Conference*, May 2007: IEEE.
[30] S. Kallio, M. Andriollo, A. Tortella, and J. Karttunen, "Decoupled d–q model of double-star interior-permanent-magnet synchronous machines," *IEEE Trans. Ind. Electron.,* vol. 60, no. 6, pp. 2486-2494, June 2013.
[31] S. Kallio, J. Karttunen, P. Peltoniemi, P. Silventoinen, and O. Pyrhönen, "Determination of the inductance parameters for the decoupled d–q model of double-star permanent-magnet synchronous machines," *IET Electr. Power Appl.,* vol. 8, no. 2, pp. 39-49, Feb. 2014.
[32] J. Karttunen, S. Kallio, P. Peltoniemi, P. Silventoinen, and O. Pyrhonen, "Decoupled vector control scheme for dual three-phase permanent magnet synchronous machines," *IEEE Trans. Ind. Electron.,* vol. 61, no. 5, May 2014.

Isaac Rudden received an MEng. degree in New and Renewable Energy Engineering from Durham University, UK, in 2020. Since 2020, he has been working toward the Ph.D. degree in electrical and electronic engineering at the University of Sheffield, U.K. His research interests include the electromagnetic design of electrical machines and renewable energy.

Peng Wang received the B.Eng. degree in electrical engineering from Nanjing Institute of Technology, Nanjing, China, in 2018 and the M.Sc. degree in electrical engineering from Southeast University, Nanjing, China, in 2021. He is currently working toward the Ph.D. degree at The University of Sheffield, Sheffield, U.K. His current research interests include sensorless control and online parameter estimation of permanent magnet synchronous machines.

Henghui Li received the B.Eng. and M.Sc. degree in electrical engineering from Zhejiang University, Hangzhou, China, in 2019 and 2022, respectively. He is currently working toward the Ph.D. degree at The University of Sheffield, Sheffield, U.K.
His current research interest includes fault detection of permanent magnet synchronous machines.

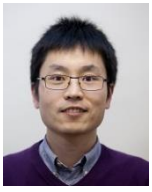

Guang-Jin Li (M'10–SM'16) received the bachelor's degree from Wuhan University, China, in 2007, the master's degree from the University of Paris XI, France, in 2008, and the PhD degree from the Ecole Normale Supérieure (ENS) de Cachan, Paris, France, in 2011, all in electrical and electronic engineering. He joined the Electrical Machines and Drives (EMD) Group, University of Sheffield, Sheffield, U.K., in June 2012, as a Postdoctoral Research Associate, where he was appointed as an Assistant Professor, in September 2013, and promoted to Associate Professor in January 2018 and Professor in January 2022. His main research interests include the design, fault diagnostics, and thermal management of electrical machines for renewable energy, automotive, and electrical aircrafts.

ZI-QIANG ZHU (M'90-SM'00-F'09) received the B.Eng. and M.Sc. degrees in electrical and electronic engineering from Zhejiang University, Hangzhou, China, in 1982 and 1984, respectively, and the Ph.D. degree in electronic and electrical engineering from the University of Sheffield, Sheffield, U.K., in 1991.,Since 1988, he has been with the University of Sheffield, where he currently holds the Royal Academy of Engineering/Siemens Research Chair and is the Head of the Electrical Machines and Drives Research Group, the Academic Director of Sheffield Siemens Gamesa Renewable Energy Research Centre, the Director of CRRC Electric Drives Technology Research Centre, and the Director of Midea Electric Machines and Controls Research Centre. His research interests include the design and control of permanent-magnet brushless machines and drives for applications ranging from automotive through domestic appliances to renewable energy. Dr. Zhu is a Fellow of Royal Academy of Engineering.

This work is licensed under a Creative Commons Attribution 4.0 License. For more information, see https://creativecommons.org/licenses/by/4.0/

This article has been accepted for publication in IEEE Access. This is the author's version which has not been fully edited and content may change prior to final publication. Citation information: DOI 10.1109/ACCESS.2024.3413145

ALEXANDER DUKE obtained M.Eng. and Ph.D. degrees in Electrical Engineering from the University of Sheffield, U.K., in 2011 and 2015, respectively. Since 2016 he has been with Siemens Gamesa Renewable Energy Research Centre where he is currently an advanced engineer specializing in the electromagnetic design of permanent magnet wind power generators.

RICHARD CLARK obtained his B.Eng. degree in Electrical Engineering from the University of Sheffield and received a Ph.D. in 1999 for research on permanent magnet actuators. Following several years as a post-doctoral Research Associate, he was awarded a 5 year Royal Academy of Engineering Research Fellowship and became a Lecturer in Electrical Engineering at the University of Sheffield in 2005. In 2007, he joined Magnomatics developing novel electrical motors and generators and magnetic transmissions, where he held posts of R&D Manager, Research Director and Principal Engineer. He joined Siemens Gamesa Renewable Energy Research Centre, Sheffield, U.K as Electromagnetic Specialist in October 2017.

This work is licensed under a Creative Commons Attribution 4.0 License. For more information, see https://creativecommons.org/licenses/by/4.0/